AMERICAN SOCIETY FOR MICROBIOLOGY | Journal of Virology®

PATHOGENESIS AND IMMUNITY

Enterovirus A71 Induces Neurological Diseases and Dynamic Variants in Oral Infection of Human SCARB2-Transgenic Weaned Mice

Jing-Yi Lin,[a,b] Kuo-Feng Weng,[c,d] Chih-Kuang Chang,[e] Yu-Nong Gong,[d,f] Guo-Jen Huang,[g,h] Hui-Lan Lee,[a] Yen-Cheng Chen,[a] Chien-Chih Huang,[a] Jia-Ying Lu,[a] Peng-Nien Huang,[d,i] Huan-Jung Chiang,[d] Che-Min Chen,[d,j] Shin-Ru Shih[d,f,k,l]

[a]Department of Clinical Laboratory Sciences and Medical Biotechnology, College of Medicine, National Taiwan University, Taipei City, Taiwan
[b]Department of Laboratory Medicine, National Taiwan University Hospital, Taipei City, Taiwan
[c]Department of Microbiology and Immunology, Stanford University School of Medicine, Stanford, California, USA
[d]Research Center for Emerging Viral Infections, College of Medicine, Chang Gung University, Taoyuan City, Taiwan
[e]Department of Laboratory Medicine, Taoyuan Chang Gung Memorial Hospital, Taoyuan City, Taiwan
[f]Department of Laboratory Medicine, Linkou Chang Gung Memorial Hospital, Taoyuan City, Taiwan
[g]Department and Graduate Institute of Biomedical Sciences, College of Medicine, Chang Gung University, Taoyuan City, Taiwan
[h]Neuroscience Research Center, Linkou Chang Gung Memorial Hospital, Taoyuan City, Taiwan
[i]Division of Infectious Diseases, Department of Pediatrics, Linkou Chang Gung Memorial Hospital, Taoyuan City, Taiwan
[j]Graduate Institute of Athletics and Coaching Science, National Taiwan Sport University, Taoyuan City, Taiwan
[k]Department of Medical Biotechnology and Laboratory Science, College of Medicine, Chang Gung University, Taoyuan City, Taiwan
[l]Research Center for Chinese Herbal Medicine, Research Center for Food and Cosmetic Safety, and Graduate Institute of Health Industry Technology, College of Human Ecology, Chang Gung University of Science and Technology, Taoyuan City, Taiwan

Jing-Yi Lin and Kuo-Feng Weng contributed equally to this work.

ABSTRACT Enterovirus A71 (EV-A71) and many members of the *Picornaviridae* family are neurotropic pathogens of global concern. These viruses are primarily transmitted through the fecal-oral route, and thus suitable animal models of oral infection are needed to investigate viral pathogenesis. An animal model of oral infection was developed using transgenic mice expressing human SCARB2 (hSCARB2 Tg), murine-adapted EV-A71/MP4 virus, and EV-A71/MP4 virus with an engineered nanoluciferase gene that allows imaging of viral replication and spread in infected mice. Next-generation sequencing of EV-A71 genomes in the tissues and organs of infected mice was also performed. Oral inoculation of EV-A71/MP4 or nanoluciferase-carrying MP4 virus stably induced neurological symptoms and death in infected 21-day-old weaned mice. *In vivo* bioluminescence imaging of infected mice and tissue immunostaining of viral antigens indicated that orally inoculated virus can spread to the central nervous system (CNS) and other tissues. Next-generating sequencing further identified diverse mutations in viral genomes that can potentially contribute to viral pathogenesis. This study presents an EV-A71 oral infection murine model that efficiently infects weaned mice and allows tracking of viral spread, features that can facilitate research into viral pathogenesis and neuroinvasion via the natural route of infection.

IMPORTANCE Enterovirus A71 (EV-A71), a positive-strand RNA virus of the *Picornaviridae*, poses a persistent global public health problem. EV-A71 is primarily transmitted through the fecal-oral route, and thus suitable animal models of oral infection are needed to investigate viral pathogenesis. We present an animal model of EV-A71 infection that enables the natural route of oral infection in weaned and nonimmunocompromised 21-day-old hSCARB2 transgenic mice. Our results demonstrate that severe disease and death could be stably induced, and viral invasion of the CNS could be replicated in this model, similar to severe real-world EV-A71 infections. We also developed a nanoluciferase-containing

Citation Lin J-Y, Weng K-F, Chang C-K, Gong Y-N, Huang G-J, Lee H-L, Chen Y-C, Huang C-C, Lu J-Y, Huang P-N, Chiang H-J, Chen C-M, Shih S-R. 2021. Enterovirus A71 induces neurological diseases and dynamic variants in oral infection of human SCARB2-transgenic weaned mice. J Virol 95:e00897-21. https://doi.org/10.1128/JVI.00897-21.

Editor Julie K. Pfeiffer, University of Texas Southwestern Medical Center

Address correspondence to Jing-Yi Lin, jingyi@ntu.edu.tw, or Shin-Ru Shih, srshih@mail.cgu.edu.tw.

Received 2 June 2021
Accepted 4 August 2021
Accepted manuscript posted online 11 August 2021
Published 13 October 2021

EV-A71 virus that can be used with this animal model to track viral spread after oral infection in real time. Such a model offers several advantages over existing animal models and can facilitate future research into viral spread, tissue tropism, and viral pathogenesis, all pressing issues that remain unaddressed for EV-A71 infections.

KEYWORDS enterovirus A71 (EV-A71), hSCARB2 transgenic mouse, *in vivo* imaging system (IVIS), quasispecies

Enterovirus A71 (EV-A71) is a neurotropic pathogen of global concern (1), and infections can cause severe central nervous system (CNS)-associated diseases, fatal neural damage, or lifelong complications in young children (2–4). The fecal-oral route is the primary route of transmission, but key questions regarding viral pathogenesis remain unanswered, such as how the virus spreads to critical organs or how the virus adapts to the complex and dynamic host environment. Several animal models have been developed to address these questions, using murine-adapted virus (5–7), immunocompromised mice (7–10), transgenic mice with viral receptor expression (9, 11–13), or even traceable virus in live infected mice (14, 15). These animal models have contributed to important discoveries (16–18), but are limited in several ways. First, most EV-A71 mouse models can only be stably infected via unnatural infection routes, such as intracerebral (i.c.), intramuscular (i.m.), or intraperitoneal (i.p.) injections (16). These routes bypass the gut region and thus may not reflect real-world viral-host dynamics. Second, several EV-A71 models of oral infection in mice use pup mice aged 1 to 7 days that are still nursing, and thus results are strongly dependent upon maternal quality of care (5, 16). In addition, Fujii et al. (11) previously reported that 3-week-old transgenic mice (transgenic mice expressing human SCARB2 [hSCARB2 transgenic mouse, clone 10; hSCARB2 Tg10]) expressing an EV-A71 receptor human scavenger receptor class B, member 2 (hSCARB2), were susceptible to oral infection by the EV-A71/Isehara strain (19); yet, although this was one of the most virulent strains tested, only 5% of infected mice experienced significant disease or death (11), suggesting inefficiencies in oral infection. Third, some models used immune-deficient animals, such as AG129 mice, which lack interferon α/β and receptor γ (8). However, interferons are important in controlling enteroviral infections and regulating innate and adapted immunity in the host intestinal region (17, 20, 21), and thus immune-deficient models may not be able to fully reflect host conditions during infection. Research into EV-A71 pathogenesis and viral-host dynamics would be greatly facilitated through the improvement of animal models, and this study presents a model of EV-A71 oral infection in 21-day-old (22) weaned hSCARB2 Tg10 mice, which aligns with the natural route of infection and is not affected by the quality of maternal care. Infected mice presented with neurological symptoms, and disease severity correlated with detected viral antigen levels in the brain. In addition, luminescent EV-A71 virus was engineered and allowed tracking of viral spread to critical organs following oral infection. EV-A71 host adaptation was also assessed through next-generation sequencing (NGS) of viral quasispecies in different tissues of infected mice. The results suggest that this model can improve upon previous models and facilitate future research into viral dynamics and pathogenesis.

RESULTS

Oral infection with murine-adapted EV-A71/MP4 virus-induced neurological symptoms and death in infected 21-day-old hSCARB2 Tg10 mice. Current animal models of EV-A71 infection generally utilize unnatural routes of infection and mice of nursing age; thus, we sought to establish a model that allows for EV-A71 oral infection of 21-day-old weaned mice. At this age, mice are sufficiently independent of their mothers to prevent confounding of results due to variations in maternal care; moreover, this age is considered to be equivalent to 1 to 2 years of human age (22), when humans are particularly susceptible to EV-A71 infection. We therefore initiated studies with hSCARB2 Tg10 mice, which carry a known EV-A71 receptor, human SCARB2, and have previously been shown to be susceptible to EV-A71 infection at 21 days of age

TABLE 1 Death in hSCARB2 mice after inoculation with EV-A71 strains

Age of mice	Route of infection	EV-A71 strain	Log_{10} PFU/mouse[a]					
			2	3	4	5	6	7
21 days	i.p.	BrCr					0/4	
		B5-12-1066					2/6	
		4643					0/7	0/7
		MP4	5/6	6/6			2/2	6/6
	i.g.	4643					0/7	
		MP4			1/7	7/11	18/21	6/6
5 mo	i.p.	4643					0/8	
		MP4					8/8	

[a]Intraperitoneal (i.p.) or intragastric (i.g.) inoculation of 21-day-old or 5-month-old hSCARB2 transgenic mice with the indicated doses of EV-A71 viral strains was conducted. Numbers indicate number of mice dying after infection/total number of inoculated mice. Blank cells indicate that the experiment was not performed.

(11). We initially tested the infectivity of our available EV-A71 strains using the i.p. route of infection. EV-A71 clinical strains BrCr, B5, and 4643, which respectively belong to EV-A71 subtypes A, B, and C (23–25), were tested, and only B5-infected mice exhibited paralysis or death following infection with 10^6 PFU of virus (Table 1). However, the murine-adapted EV-A71/MP4 strain, which was derived from the EV-A71/4643 clinical isolate and contains 35 nucleotide and 5 amino acid changes (6), exhibited significantly greater infectivity than its parental strain, with 100 PFU and 1,000 PFU of inoculate, respectively, inducing severe disease and death in 83% (5/6) and 100% (6/6) of infected mice (Table 1). Moreover, 100% (6/6) mortality rates were observed in 5-month-old adult mice that received 10^6 PFU of the EV-A71/MP4 strain (Table 1). We assessed whether the high pathogenicity of the EV-A71/MP4 strain would facilitate oral infection of hSCARB2 Tg10 mice. As weanling mice were still incapable of ingesting water stably, we elected to perform virus inoculation by gavage for all of our oral infection experiments to ensure that each mouse can receive the same level of virus loading. Intragastric inoculation by gavage with 10^4, 10^5, 10^6, and 10^7 PFU of virus subsequently induced 14% (1/7), 63% (7/11), 85% (18/21), and 100% (6/6) mortality rates in infected mice, with most dying 6 days postinfection (dpi) (Fig. 1A). Neurological symptoms (limb weakness and paralysis) in infected mice were monitored and scored as 0, 1, 2, 3, and 4, respectively, indicating healthy status, weakness in a limb, paralysis of a single limb, paralysis of two or more limbs, and death (Fig. 1C). Mice infected with 10^6 to 10^7 PFU of EV-A71/MP4 virus began to present neurological symptoms (disease score [DS] $>$ 1) at 4 to 5 dpi, whereas animals infected with 10^4 to 10^5 PFU began presenting neurological symptoms at 7 to 8 dpi (Fig. 1C and D). Of the 10^7 PFU-inoculated mice, 50% (3/6) died before presenting neurological symptoms, suggestive of an overdose infection. Incidentally, no disease or death was seen in hSCARB2 mice orally inoculated with 10^6 PFU of the EV-A71/4643 parental strain (Fig. 1A and Table 1) or in 21-day-old wild-type C57BL/6 mice (without hSCARB2) orally inoculated with 10^6 PFU of the EV-A71/MP4 strain (Fig. 1B). These results confirm that murine-adapted EV-A71/MP4 virus can infect 21-day-old weaned mice through the natural oral route of infection, and infected mice present with neurological symptoms and death comparable to severe infections in humans.

EV-A71/MP4 virus detected in the CNS of orally infected hSCARB2 Tg10 mice. To determine whether the EV-A71/MP4 virus can invade the CNS following oral infection, 21-day-old hSCARB2 Tg10 mice were gavaged with 10^6 PFU of virus, and their brains and spinal cords were harvested at 1 to 5 dpi. Considerable amounts of viral genomic RNA were detected in the brains (Fig. 1E) and spinal cords (Fig. 1F) of infected mice at 3 and 5 dpi, respectively. We further performed immunostaining of the viral VP1 antigen within the brains of mock or EV-A71/MP4-infected mice (10^6 PFU per mouse) at 6 dpi and also recorded the disease scores (DS) of each mouse on the days

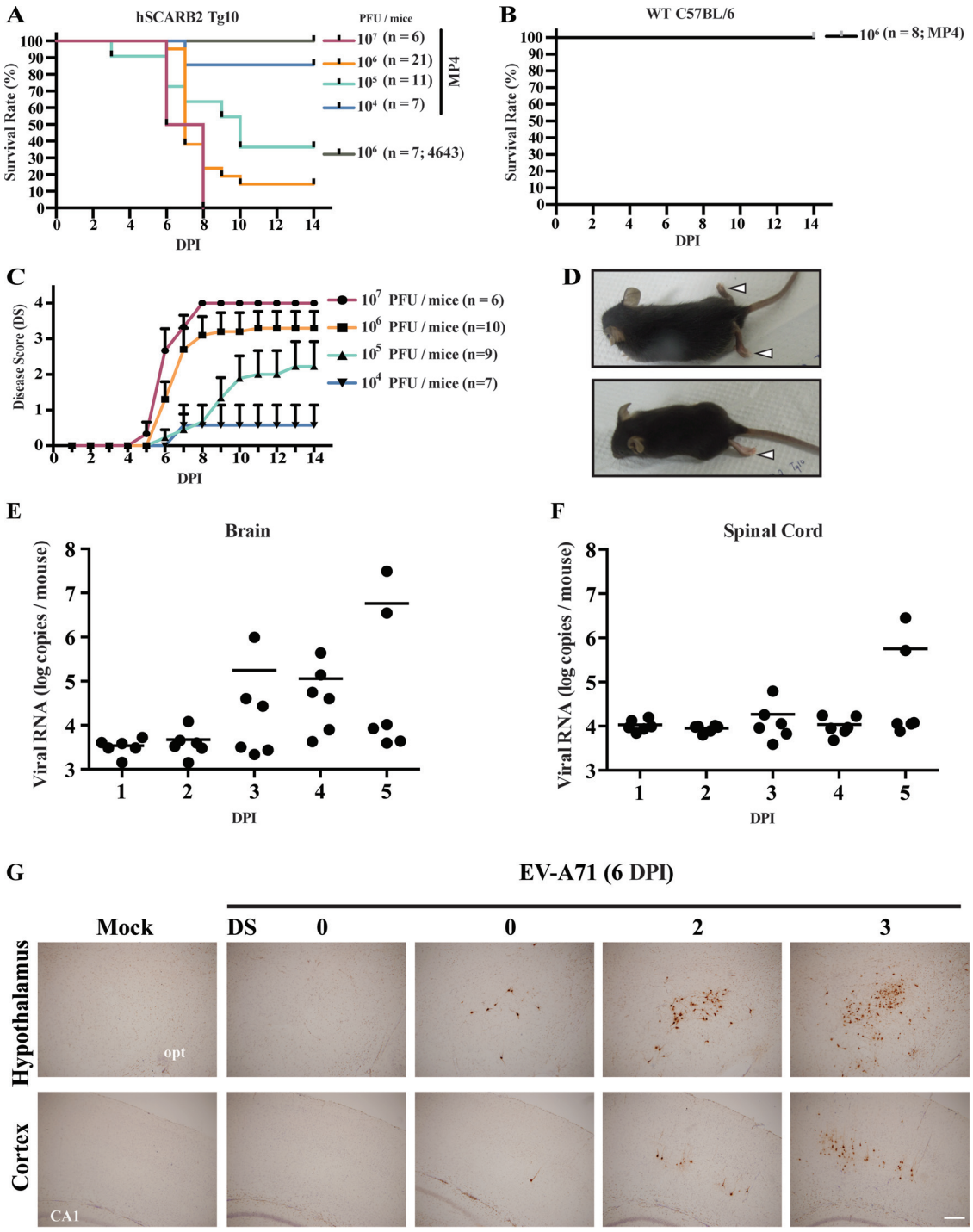

FIG 1 Pathogenesis of EV-A71 in mice. Survival curves of 21-day-old hSCARB2 Tg10 mice (A) or control wild-type C57BL/6 mice (B) orally inoculated with murine-adapted EV-A71/MP4 virus or its EV-A71/4643 parental strain. Mice were intragastrically (i.g.) inoculated with a specified number of PFU of each virus strain and then monitored daily for 14 days postinfection (dpi). (C) Neurological diseases in 21-day-old hSCARB2 transgenic mice inoculated i.g. with the indicated PFU of EV-A71/MP4. Diseases were monitored daily until 14 dpi and scored as follows: 0 = healthy, 1 = weakness of a limb, 2 = paralysis of a single limb, 3 = paralysis of two or more limbs, 4 = death. (D) Limb paralysis (white arrowheads) in hSCARB2 Tg mice infected with 10^5 PFU (top panel) or 10^6 PFU (bottom panel) of EV-A71/MP4 at 9 and 7 dpi, respectively. Viral genomic RNA levels in the brains (E) and spinal cords (F) of EV-A71/MP4-infected hSCARB2 Tg10 mice, which were harvested on the specified dpi. (G) EV-A71 capsid protein (VP1) expression in the hypothalamus and cortex of mock or orally infected (10^6 PFU of EV-A71/MP4) hSCARB2 mice at 6 dpi. Disease scores (DS) of observed neurological diseases in infected mice are indicated. Scale bar = 200 μm. CA1, hippocampal CA1; opt, optic nerve.

when brains were harvested. The results showed that the viral VP1 antigen was predominantly located in the hypothalamus and cortex of the brain in infected mice (Fig. 1G). Mice with higher viral antigen levels in the brain presented with more severe neurological symptoms as indicated by disease scores (Fig. 1G). These results suggest that the oral route of infection allows the EV-A71/MP4 virus to invade the CNS and induce neurological disease.

Development of bioluminescent EV-A71-MP4-Nluc5 reporter virus. We sought to understand how the EV-A71/MP4 virus spreads in the host following oral infection, and previous work by Caine and Osorio confirmed that a nanoluciferase-carrying EV-A71 virus can emit bioluminescence in infected cells and stably reflect viral spreading in the tissues of i.p. inoculated mice (14). However, it is unclear whether this would apply in the context of an oral infection murine model. We therefore proceeded to construct an EV-A71-MP4-Nluc5 reporter virus cDNA clone by engineering the nanoluciferase gene in the infectious cDNA clone, pCR-XL-TOPO-EV-A71-MP4 (Fig. 2A), and used this as a template to generate viral RNA by *in vitro* transcription. We subsequently recovered the EV-A71-MP4-Nluc5 recombinant virus from viral RNA-transfected rhabdomyosarcoma (RD) cells and confirmed that the recovered virus can successfully infect RD cells and generate 1-mm-wide plaques in a 4-day incubated plaque assay (Fig. 2B). We further compared the plaque morphology and growth kinetics of the EV-A71/MP4 and EV-A71-MP4-Nluc5 viruses and found that the plaque size of EV-A71-MP4-Nluc5 was smaller than that of EV-A71/MP4 (Fig. 2B) and that viral titers of EV-A71-MP4-Nluc5 were lower than those observed for EV-A71/MP4 (Fig. 2C). We then evaluated nanoluciferase activity in infected cells at different hours postinfection, and the results indicated that activity increased over time (Fig. 2D). To assess the stability of EV-A71-MP4-Nluc5, the virus was passaged 15 times on RD cells. Nanoluciferase activity was maintained at 5 passages but was subsequently lost from the virus after 10 passages (Fig. 2E). Viral 3D, 3CD, and P3 protein expression levels were also assessed at passages 2, 5, 10, and 15 to serve as positive controls, and no significant difference in viral protein expression levels was noted between these points (Fig. 2F).

Oral infection with EV-A71-MP4-Nluc5 virus induces neurological symptoms in hSCARB2 Tg10 mice. The nanoluciferase-carrying EV-A71 virus reported by Caine and Osorio is attenuated and failed to induce symptoms in i.p. inoculated 3-week-old mice (14). We orally infected 21-day-old hSCARB2 Tg10 mice with varying titers of our newly constructed EV-A71-MP4-Nluc5 virus and then recorded change in body weight (Fig. 3A), neurological disease scores (Fig. 3B), and survival rates (Fig. 3C) on a daily basis until 12 dpi. Results showed that oral infection with weaned hSCARB2 Tg10 mice with 2.8×10^7, 2.8×10^8, and 5.6×10^8 PFU of EV-A71-MP4-Nluc5 virus, respectively, induced death in 10% (1/10), 80% (8/10), and 100% (10/10) of infected mice (Fig. 3C). As with EV-A71/MP4 oral infections (Fig. 1), mice infected with EV-A71-MP4-Nluc5 virus began to present with neurological symptoms or death at 5 to 6 dpi (Fig. 3B and C), and symptoms were reflected in weight loss as well (Fig. 3A). These results confirm that oral inoculation of EV-A71-MP4-Nluc5 virus is viable and causes similar disease patterns and severity as EV-A71/MP4 oral infections in weaned hSCARB2 Tg10 mice.

Real-time *in vivo* imaging of EV-A71-MP4-Nluc5 viral spread. Following oral infection (intragastrically [i.g.]) of hSCARB2 Tg10 mice with 5.6×10^8 PFU of EV-A71-MP4-Nluc5 virus, we tracked bioluminescent signals at 1 to 4 dpi. From the ventral view, we observed that bioluminescence mostly located to the gastrointestinal (GI) tract at 2 dpi, but over the next 2 days (3 to 4 dpi), the signals spread to other organs in the chest while declining in the gastrointestinal region (Fig. 4A). From the dorsal view, bioluminescence was observed in the head at 2 dpi and persisted until the last day of imaging (4 dpi); we also observed strong signals in the upper and lower back at 2 dpi and then only in the upper back at 3 to 4 dpi (Fig. 4A). Incidentally, when bioluminescence was observed in infected mice, significant weight loss was also noted, even though significant limb paralysis was not seen until 4 dpi (Fig. 4A). We subsequently collected the brain, spinal cord, stomach, intestine, liver, spleen, heart, lung, and both forelimb and hindlimb muscles from the same infected mouse at 4 dpi after the last

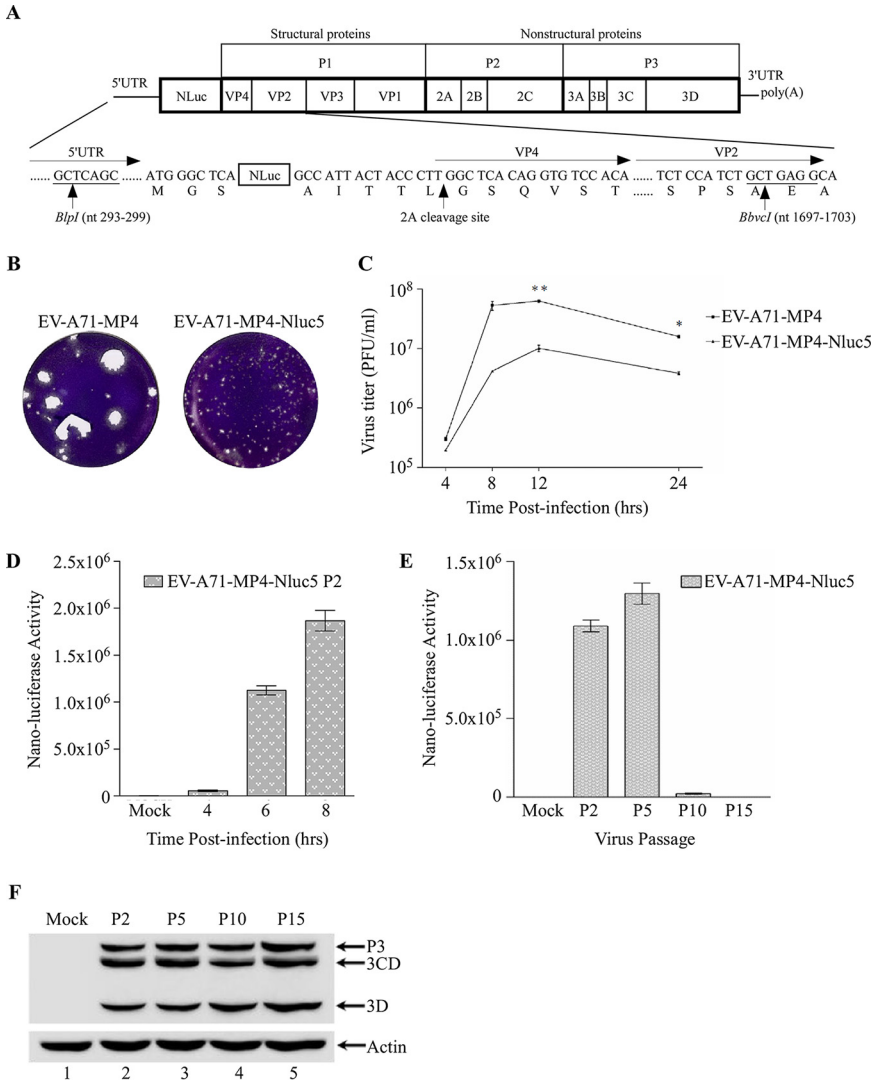

FIG 2 Construction and characterization of the EV-A71-MP4-Nluc5 reporter virus. (A) An infectious cDNA clone, pCR-XL-TOPO-EV-A71-MP4, was used as the backbone, and the nanoluciferase reporter gene was inserted between the 5′ UTR and VP4 sequences. The 2A protease cleavage site (ITTLG) is indicated by an arrow. (B) Plaque morphology of EV-A71/MP4 and EV-A71-MP4-Nluc5 in RD cell cultures. (C) Viral growth of EV-A71/MP4 and EV-A71-MP4-Nluc5. RD cells were infected with a multiplicity of infection (MOI) of 10 for the EV-A71/MP4 or EV-A71-MP4-Nluc5 virus, and virus titers were detected by plaque assay. (D) Nanoluciferase activity of EV-A71-MP4-Nluc5 virus. RD cells were infected with a multiplicity of infection of 10 for the EV-A71-MP4-Nluc5 virus, and cell lysates were collected at the stated times for assessment of nanoluciferase activity. (E) Summary of nanoluciferase activity at different EV-A71-MP4-Nluc5 passages. RD cells were infected with an MOI of 10 for the EV-A71-MP4-Nluc5 virus of the indicated passages, and cell lysates were collected at the stated times for assessment of nanoluciferase activity. (F) Summary of viral protein (P3, 3CD, and 3D) expression levels at different EV-A71-MP4-Nluc5 virus passages. RD cells were infected with an MOI of 10 for the EV-A71-MP4-Nluc5 virus of the indicated passages, and cell lysates were collected to assess viral protein expression levels by Western blotting.

imaging and performed immunostaining to evaluate the presence of EV-A71 viral capsid protein (VP1) in these collected tissues. Results revealed intensive VP1 staining in the brain, spinal cord, lung, and forelimb muscle; reduced staining in the stomach, intestine, liver, and hindlimb muscle; and none in the heart (Fig. 4B). These results confirm that our constructed EV-A71-MP4-Nluc5 virus can be used to track viral spread in this model of oral infection.

EV-A71 genetic diversity in different tissues of infected mice. The low fidelity of enterovirus replication contributes to genetically diverse viral populations that increase

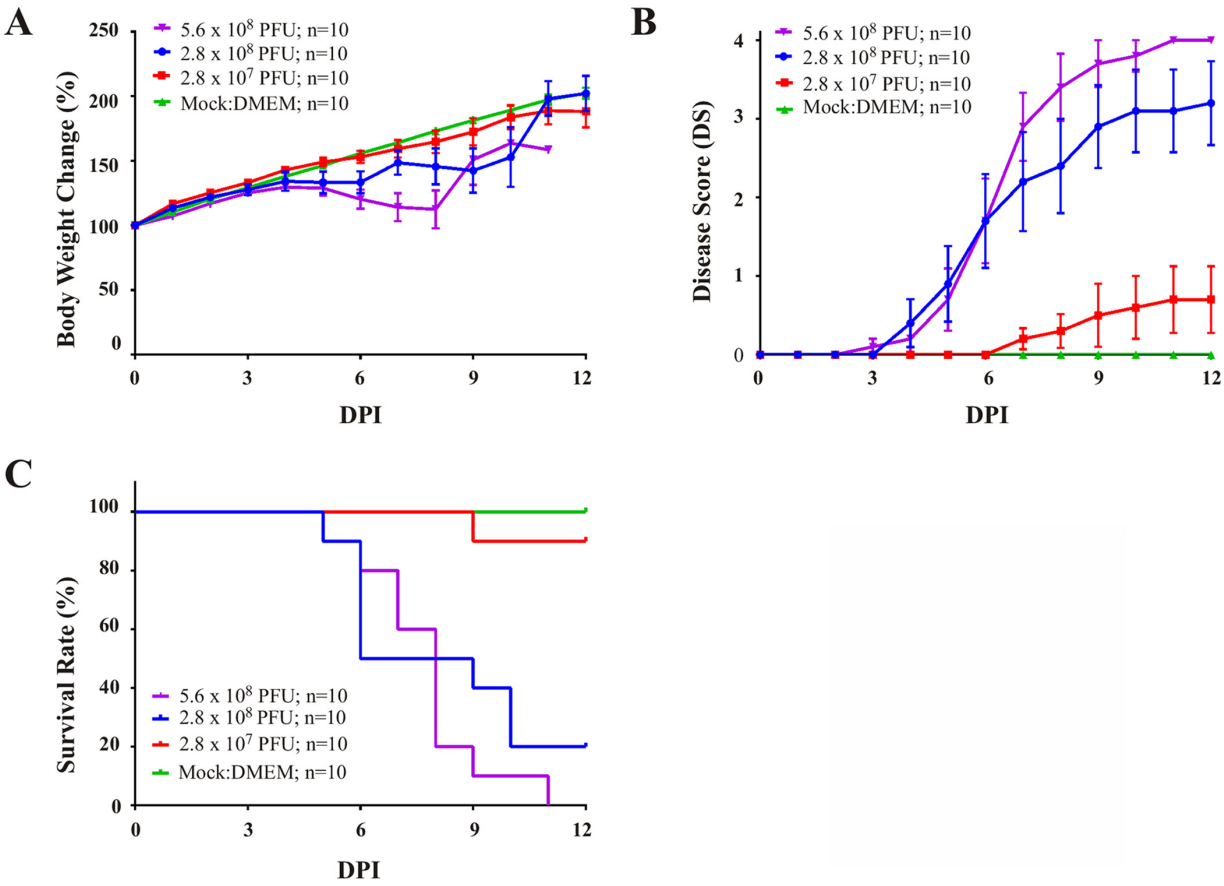

FIG 3 EV-A71-MP4-Nluc5 virus infection in 21-day-old hSCARB2 Tg10 mice. (A) Body weight change in 21-day-old hSCARB2 Tg10 mice orally inoculated with the specified PFU of EV-A71-MP4-Nluc5 virus and then monitored daily for 12 dpi. (B) Neurological symptoms in 21-day-old hSCARB2 Tg10 mice orally inoculated with the indicated PFU of EV-A71-MP4-Nluc5 virus. Disease score was monitored daily until 12 dpi as follows: 0 = healthy, 1 = weakness of a limb, 2 = paralysis of a single limb, 3 = paralysis of two or more limbs, and 4 = death. (C) Survival rates of 21-day-old hSCARB2 Tg10 mice orally inoculated with the indicated PFU of EV-A71-MP4-Nluc5 virus.

the chance of viral adaptation and spread in a complex host environment (26–28). Different routes of infection may provide varying selective pressures that impact this process (29). Previous studies have shown that bottlenecks in mice that were orally infected with poliovirus or coxsackie B3 virus subsequently affected the diversity of disseminated virus in various tissue (30, 31). However, the selective pressures upon EV-A71 genomes in an orally infected animal model have not been documented as yet. We therefore used NGS to analyze viral genome sequences derived from different organs of an hSCARB2 Tg10 mouse orally infected with EV-A71-MP4-Nluc5 virus. The brain, spinal cord, heart, lung, stomach, intestine, forelimb muscle, hindlimb muscle, spleen, liver, kidney, and blood were harvested from the infected mouse at 3 dpi when it presented neurological symptoms (disease score = 1), and total RNA was extracted from these organs for NGS analysis. NGS coverage and average depths from 12 different organs were further calculated, eventually achieving more than 88% of read coverage, except for the kidney and liver (Fig. 5A). To further investigate dynamic populations of minor variants using sufficient reads, five samples (including the lung, spinal cord, brain, heart, and blood) with $>200\times$ NGS depth were selected, and minor variants (by percentage) at sites with $>200\times$ in these five samples are shown in Fig. 5B. A total of five variants were identified with at least 25% minor nucleotide population and $200\times$ depth, including two synonymous substitutions (VP1-V69 and VP1-E213) and one substitution at position 597 of the 5′ untranslated region (UTR) identified in the spinal cord and two nonsynonymous substitutions (VP1-A188T and 3B-K8N) identified

A

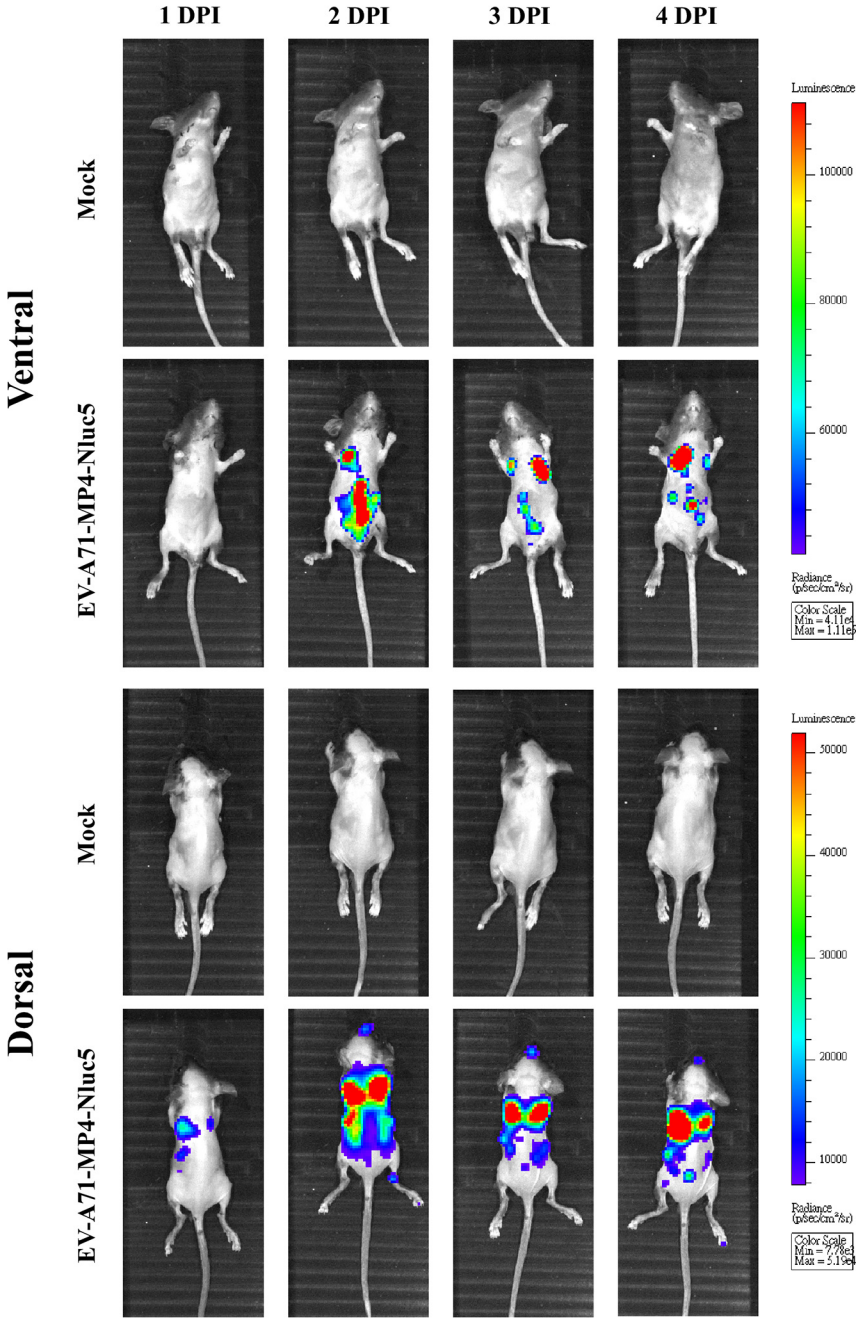

DPI		1	2	3	4
Body Weight change (%)	Mock	95	103	112	117
	EV-A71-MP4-Nluc5	89	82	76	76
Disease Score (DS)	Mock	0	0	0	0
	EV-A71-MP4-Nluc5	0	0	0	0

FIG 4

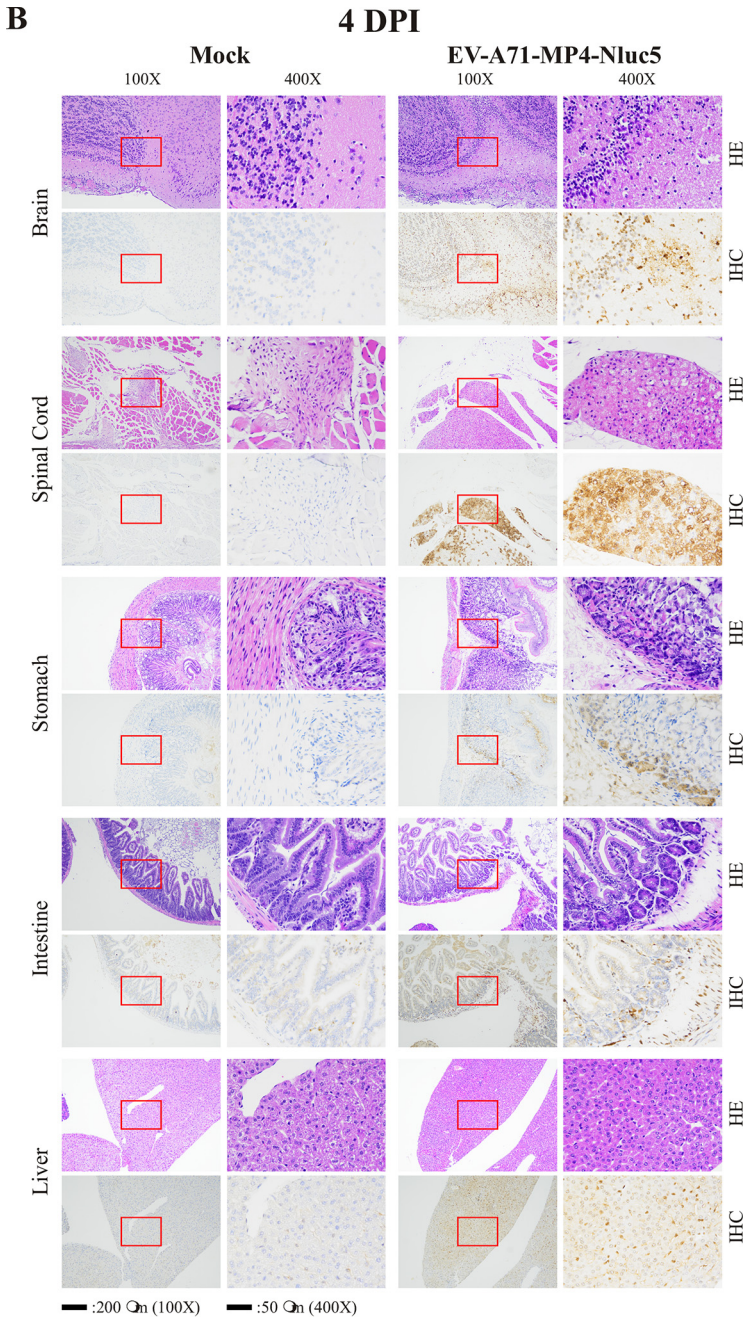

FIG 4

in the blood. Table 2 presents the nucleotide compositions of these five variants. A percentage of 31.35% for the VP1-V69 variant identified in the spinal cord equals a count of 2,339 reads with the minor nucleotide alphabet (C) divided by a total of 7,460 reads. In other words, these five variants with more than 200× the total depth were located where the primary nucleotide alphabet dominated less than 75%.

DISCUSSION

This study presents an animal model of EV-A71 infection that utilizes the natural route of oral infection in weaned and nonimmunocompromised 21-day-old hSCARB2 Tg10 mice. Results showed that severe disease and death could be stably induced (Fig. 1A to D and Fig. 3), and viral invasion of the CNS could be replicated (Fig. 1E and F and

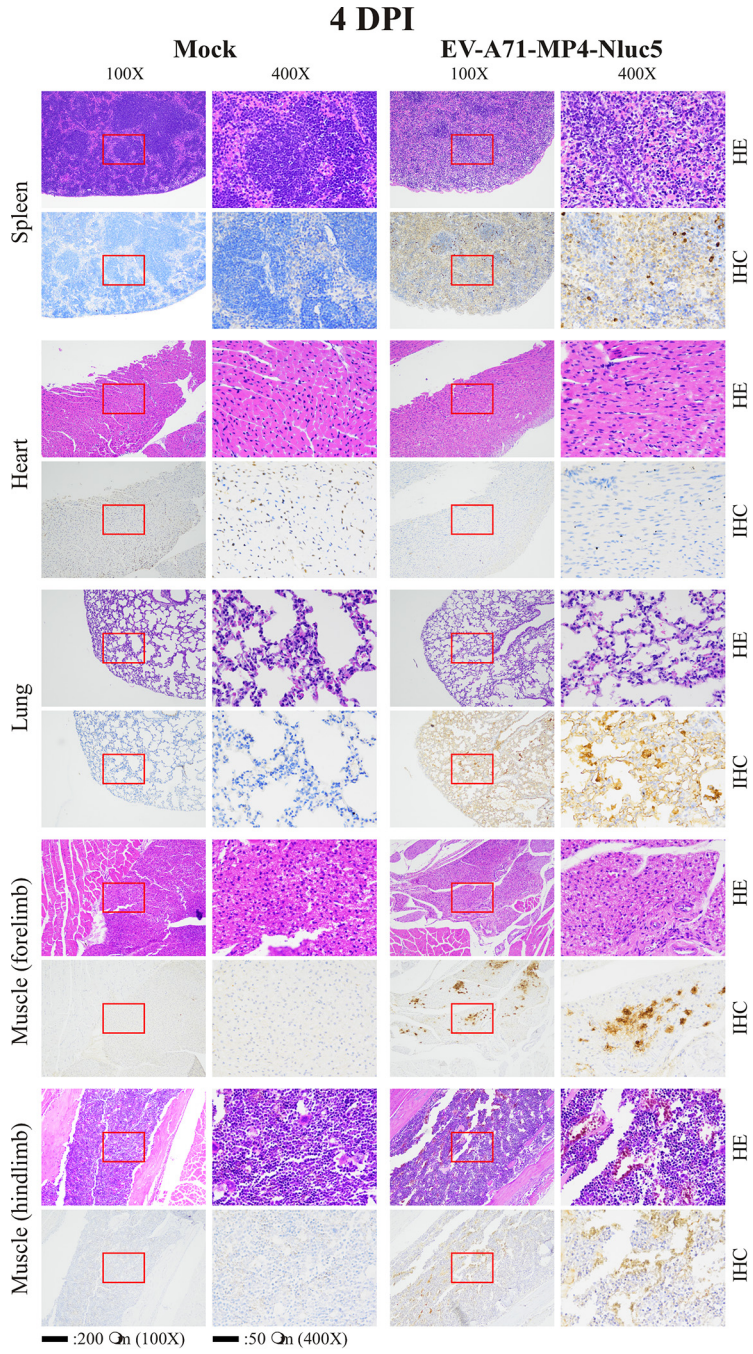

FIG 4 Real-time *in vivo* imaging of EV-A71-MP4-Nluc5 infection. (A) Ventral and dorsal views of hSCARB2 Tg10 mice after infection with EV-A71-MP4-Nluc5. Viral spread was monitored in real-time after 5.6×10^8 PFU of the virus was intragastrically inoculated into 21-day-old hSCARB2 Tg10 mice. Bioluminescence was visualized in the brain of infected hSCARB2 Tg10 mice at 2 days postinfection. Luminescence was undetected in hSCARB2 Tg10 mice (mock), which served as a negative control. The body weight of EV-A71-MP4-Nluc5-infected mice decreased, even without visible disease symptoms at 1 to 4 dpi. Histopathological changes and viral antigen (VP1) expression in different organs of 21-day-old hSCARB2 Tg10 mice i.g. inoculated with 5.6×10^8 PFU of EV-A71-MP4-Nluc5 at 4 dpi, with the brain, spinal cord, stomach, intestine, liver, spleen, heart, lung, muscle (forelimb), and muscle (hindlimb) shown in panel B. HE, hematoxylin and eosin stain; IHC, immunohistochemistry staining.

Fig. 4B) with neurological symptom severity correlating with viral antigen levels (Fig. 1G). We also developed a nanoluciferase-containing EV-A71 virus that can be used to track viral spread after oral infection in real time (Fig. 4). Such a model offers several advantages. With the use of 21-day-old weaned mice, survival rates are no longer

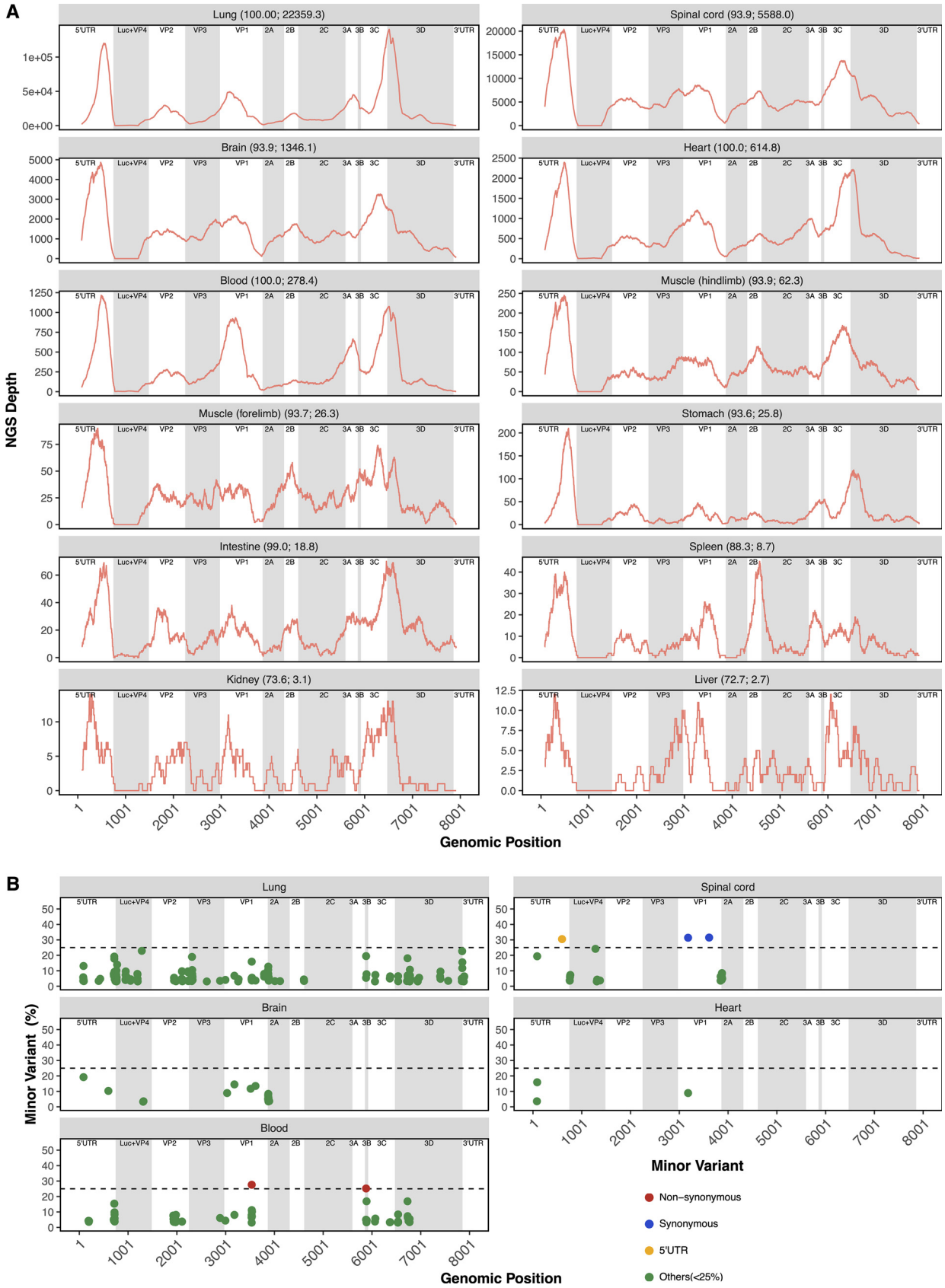

FIG 5 Genetic diversity of EV-A71-MP4-Nluc5 derived from different organs of infected mice. Following intragastric inoculation of 21-day-old hSCARB2 Tg10 mice with 5.6×10^8 PFU of EV-A71-MP4-Nluc5 virus, the brain, spinal cord, heart, lung, stomach, intestine, forelimb muscle,

(Continued on next page)

TABLE 2 Next-generation sequencing depth and nucleotide composition in genomic positions with minor variants

Source	Genomic position	Amino acid position of gene[a]	Nucleotide in reference	Minor variant (%)	Total depth	Count of A/G/C/T/Del
Spinal cord	597	5′ UTR-597[b]	G	C (30.47)	11,292	6/7,838/3,441/5/2
Spinal cord	3181	VP1-V69	T	C (31.35)	7,460	2/5/2,339/5,114/0
Blood	3536	VP1-A188T	G	A (27.56)	283	78/182/7/5/11
Spinal cord	3613	VP1-E213	A	G (31.53)	4,310	2,950/1,359/1/0/0
Blood	5881	3B-K8N	G	T (25.20)	393	7/285/2/99/0

[a]Synonymous mutation, VP1-V69 and VP1-E213; nonsynonymous mutation, VP1-A188T and 3B-K8N.
[b]Nucleotide position in untranslated region according to the reference strain.

confounded by the quality of maternal care, and this age is also considered to be equivalent to 1 to 2 years of human age (22), when humans are highly susceptible to EV-A71 infection. In addition, the development of a nanoluciferase-containing EV-A71 virus allows us to observe virus spreading within this oral infection model and reduces the need for mice as well as the time and effort involved in tissue harvesting and analyses. The ability to observe bioluminescent signals of viral spread along with disease symptoms in real time (Fig. 3 and 4) is valuable for research.

Caine and Osorio have shown that the insertion of a bioluminescent gene into their mouse-adapted EV-A71 (mEV71) resulted in attenuation of the virus in infecting AG129 mice (14, 15). Intraperitoneal injection of 2.4×10^6 PFU of wild-type mEV71 killed all of the infected mice within 20 days postinfection, but infection with NLuc-mEV71 at the same titers not only failed to kill any mouse but also did not induce any clinical signs in infected mice. Similar attenuation was observed in our luciferase-carrying EV-A71 (EV-A71-MP4-Nluc5). Intragastric inoculation of EV-A71-MP4-Nluc5 required 100-fold higher viral titers than wild-type EV71/MP4 before comparable death rates in infected mice were observed (Fig. 3), and in order to observe viral spreading and clinical signs that would be reflective of mice infected with wild-type EV71/MP4, we opted to inoculate mice with titers of EV-A71-MP4-Nluc5 that could kill 100% of mice (5.4×10^8 PFU per mouse). The virus spreading pattern seen with infected mice in our oral infection model showed several differences from the i.p. infection model described by Caine and Osorio (14). First, our orally infected mice showed temporarily increased replication in the abdominal region at 2 dpi, which quickly diminished and moved to the chest and upper region from 3 dpi; however, Caine and Osorio showed steady viral replication within the abdomen during the first 5 dpi. Second, we did not observe viral replication signals from the footpads of infected mice as described by Caine and Osorio. Third, the high viral titers that we used caused infected mice to die quickly and thus prevented us from observing the persistent infections noted by Caine and Osorio. These differences may stem from different routes of infection, virus strains, mouse species, and viral titers used for inoculation. Further investigation of these differences and the underlying mechanisms would certainly help to optimize the study of EV-A71 viral spread following natural-route infection.

Oral infection experiments are usually performed by oral or gavage (intragastric) inoculation (32). A previous study has reported oral inoculation of adult poliovirus receptor (PVR)-transgenic mice (6 to 7 weeks old) with poliovirus by feeding them from a virus-containing drinking water bottle (33), but the EV-A71-susceptible mice used in this study were younger than 3 weeks, and their ability to ingest water from a bottle was limited. As oral inoculation methods were unsuited for this study, we duly elected to perform gavage inoculation, and there is precedence for this in previous EV-A71 studies (5, 11). The gavage procedure offers additional advantages in that viral titers

FIG 5 Legend (Continued)
hindlimb muscle, spleen, liver, kidney, and blood were harvested from the infected mouse at 3 dpi when neurological symptoms presented (disease score = 1). Total RNAs from these organs were extracted and analyzed by next-generation sequencing (NGS). (A) NGS depths of the EV-A71 genome from different organs of infected mice. (B) Single-nucleotide variants detected in EV-A71-MP4-Nluc5 harvested from different organs in infected mice. Single-nucleotide variants of the EV-A71 genome untranslated and protein-coding regions in different organs were plotted by nucleotide position.

can be better controlled, and accidental inoculation of virus in other sites (such as the respiratory tract) can be avoided. We therefore chose to follow the methods described in previous EV-A71 studies to conduct gavage procedures for all of our oral infection experiments in this study.

Enterovirus infections have been hypothesized to begin in the gastrointestinal (GI) tract (33), but questions regarding viral-host interactions in the GI region remain unanswered, possibly because of the limitations in current infection models, which utilize unnatural infection routes such as i.c., i.m., or i.p. inoculation, thereby allowing the virus to skip the initial infection stage in the GI tract. By contrast, our model mimics the natural route of infection, and we further demonstrate that the murine-adapted EV-A71/MP4 virus can spread from the GI tract to the CNS to induce neurological disease, suggesting that this model may better replicate severe infections in humans. Moreover, the innate immune response is critical for the control of enterovirus infection and pathogenesis (17, 20), and interferons play an important role in regulating innate and adaptive immunity in the GI region upon viral infection (21). Whereas previous enterovirus models have relied on the use of immunocompromised mice (7–10, 34), the hSCARB2 Tg10 mice used in this study are nonimmunocompromised, and thus this model can help to address questions regarding EV-A71 viral interactions with the gut immune response.

The low fidelity of enteroviral genome replication helps EV-A71 to overcome the pressures of the complex and dynamic host environment, including GI barriers, host immune responses, and other factors, such as receptor-binding requirements (19, 35–40), by generating diverse quasispecies (26–29). Many research groups have identified various enteroviral genomes crucial for viral adaptation (41–43), and it is expected that different routes of infection will affect these dynamics differently; for example, it is known that intravenous (i.v.) or i.c. inoculation of poliovirus facilitates viral spread to the brain over i.p. inoculation in murine models (29). In our oral infection model, the 100% lethal dose (LD_{100}) of oral infection with EV-A71/MP4 virus was 1,000-fold higher than i.p. infection (Table 1), suggesting that this model preserves selective pressures that are specific to the oral route, similar to those encountered during a real-world infection. However, little is known about how EV-A71 overcomes these pressures during a natural-route infection, and therefore we conducted NGS analysis of viral genomes collected from different host organs to shed light upon this issue. We found high ratios of viral variants in the brain, spinal cord, and lung of orally infected mice, with diverse mutations concentrated within the 5′ UTR, VP1, and 3B regions of the viral genome (Fig. 5). The results suggest that these regions may be important for viral spread and pathogenesis, and further investigation is warranted. The internal ribosome entry site (IRES) region of enterovirus plays an important role in viral translation. In poliovirus, the crucial attenuating Sabin mutations have been mapped to PV IRES dV at nucleotides 480, 481, and 472 in the Sabin 1, Sabin 2, and Sabin 3 strains, and these mutations can inhibit viral translation in cells of the host central nervous system (44). We identified a 5′-UTR 597 variant from the spinal cord, and further investigation on the pathogenesis of this variant is ongoing. Enterovirus VP1 plays an important role in receptor binding, and previous research shows that variants can affect virulence and pathogenesis (42). We identified a VP1-A188T variant from the blood and will investigate whether this variant affects viral-host receptor binding. The EV-A71 3B protein, also known as VPg (virus genome-linked protein), is a nucleic acid chaperone protein comprising 22 amino acids and is covalently linked with the 5′ terminus of the EV-A71 genome through a 5′-tyrosyluridine bond in the conserved tyrosine residue of VPg (45). VPg can be uridylylated to form VPg-pUpU, which participates in the initiation of RNA replication. We identified a 3B-K8N variant in the blood and will further investigate whether this variant affects viral RNA replication and pathogenesis.

In conclusion, this work presents an efficient model of EV-A71 oral infection in weaned and nonimmunocompromised 21-day-old hSCARB2 Tg10 mice, with strong potential to facilitate future *in vivo* research regarding the dynamics of viral replication and spread, quasispecies formation, tissue tropism, and pathogenesis.

MATERIALS AND METHODS

Cells and viruses. Rhabdomyosarcoma (RD) cells were maintained in Dulbecco's modified Eagle's medium (DMEM) (Invitrogen, CA) supplemented with 10% fetal bovine serum (FBS) (Gibco, NY). Cells were maintained at 37°C in 5% CO_2. EV-A71/BrCr (23) was purchased from the ATCC. EV-A71/B5 was isolated in 2012 from Chang Gung Memorial Hospital (24). EV-A71/4643/98, EV-A71/MP4, and EV-A71-MP4-Nluc5 were generated from infectious clones as previously reported (6). All EV-A71 viruses were amplified using RD cells. To ensure the stable infectivity of EV-A71 in mice, all viruses used for murine infection were harvested only from the first amplification of the virus generated in viral RNA-transfected RD cells.

Construction of plasmids. An infectious cDNA clone, pCR-XL-TOPO-MP4, was utilized as the backbone for construction of the EV-A71 MP4-NLuc reporter virus. The NanoLuc luciferase (NLuc) gene was inserted between the 5′ UTR and the VP4 gene (Fig. 2A), and an EV-A71 2A protease cleavage sequence (CTTG) was placed immediately after the NLuc coding sequence.

Virus recovery from full-length infectious cDNA was completed for NLuc constructs. cDNAs were linearized with MluI, and full-length RNA transcripts were synthesized using a MEGAscript T7 transcription kit (Thermo Fisher Scientific, MA) per manufacturer's instructions. RD cells were transfected with 1 μg of RNA transcripts. Once a 90% cytopathic effect was observed, the virus was collected and titrated by plaque assay. Viral RNA was extracted from recovered virus and sequenced to ensure that the virus and NLuc sequences were correct.

Mice. The hSCARB2 Tg10 mice were kindly provided by Satoshi Koike of the Tokyo Metropolitan Institute of Medical Science, Japan (11) and feed by the National Laboratory Animal Center (NLAC), NARLabs, Taiwan. Wild-type C57BL/6 mice were obtained from BioLASCO (Taiwan). All mice were bred and maintained in specific-pathogen-free environmentally controlled rooms at 25 $\pm$ 1°C.

Viral infection of mice. Indicated EV-A71 viral strains were injected intraperitoneally (i.p.) or intragastrically (i.g.) to infect 21-day-old hSCARB2 Tg10 mice or 5-month-old wild-type C57BL/6 mice, after which disease scoring and change in body weight was monitored daily for all mice until death or 14 dpi. Intragastric infection was performed by gavage, in which we prepared virus solution in DMEM at the indicated viral titers and used a 25-G feeding needle to gavage a total of 100 μl of virus solution into the mice following 24 h of fasting. *In vivo* imaging was conducted on groups (n = 6) of 21-day-old hSCARB2 Tg10 mice that received 100 μl of i.g. injection with 4 $\times$ 10^6 PFU/ml of EV-A71-MP4-NLuc as well as control groups that received 100 μl of DMEM instead. Weight loss, disease score, and survival were recorded, and for imaging, Nano-Glo reagent was diluted 1:20 in 1$\times$ phosphate-buffered saline (PBS) and then immediately injected (100 μl) into anesthetized mice. An IVIS 200 imaging system (PerkinElmer, MA) was used to capture images, which were analyzed using Living Image software (PerkinElmer).

Tissue harvesting and staining. Sacrificed mice were perfused with 4% paraformaldehyde at pH 7.4, with brains removed and postfixed overnight, and then dehydrated for 24 h in 25% sucrose solution. Coronal sections were cut at a thickness of 40 μm, and sections were placed in an antifreeze bath (1:1:2 glycol, ethylene glycol, PBS). Sections were mounted on Superfrost slides and dried overnight, incubated in 0.01 M citric acid for 10 min at 90°C, and then incubated in 3% H_2O_2 for 10 min, rinsed in 1$\times$ PBS, and incubated overnight at room temperature in mouse anti-enterovirus A71 antibody (MAB979; MilliporeSigma, MA) for enterovirus A71 staining. On the following day, a standard IgG ABC kit (Vector Labs, CA) procedure was used, and the slides were reacted for 5 to 10 min with 3,3′-diaminobenzidine. Sections were then counterstained with cresyl violet and cover-slipped under DPX mounting medium.

Quantitative RT-PCR to determine viral genomic RNA levels in tissues. Mice tissues were homogenized in DMEM and centrifuged at 12,000 $\times$ *g*. RNA in the supernatant was isolated using a LabTurbo 48 compact system, and purified RNA samples were treated with DNase I (Promega, WI) and used as templates for ReverTra Ace (Toyobo, Japan) cDNA synthesis. The cDNA was detected using KAPA SYBR Fast qPCR master mix (KAPA Biosystems) and primers targeting the 5′ UTR region of the EV-A71 genome, 5′-CCCTGAATGCGGCTAATC-3′ and 5′-ATTGTCACCATAAGCAGCCA-3′. Real-time reverse transcription-quantitative PCR (RT-PCR) amplifications were carried out using ABI 7500 (Applied Biosystems, CA). The standard curve for calculating viral genome copy numbers was plotted using plasmid DNA containing the EV-A71 genome (EV-A71/MP4 infectious clone) and quantitative real-time PCR.

NGS analysis. NGS data analysis was performed using HiSeq (Illumina, CA). Raw data was trimmed to remove short and low-quality reads using Trimmomatic version 0.39, after which quality reads were mapped to the mouse GRCm38 reference genome to remove the host genome using HISAT2 version 2.1.0. The remaining reads were mapped to our reference sequence using bowtie2 version 2.4.2 (default setting with very-sensitive option). SAMtools with an option of disabling per-base alignment quality (BAQ) computation was applied to calculate read counts and variant frequencies and generate the pileup file (46, 47). We respectively trimmed genomic positions 1 to 80 in the 5′ end genome and 7915 to 7994 in the 3′ poly(A) tail in order to eliminate variants generated by sequencing bias. Figure 5A shows read coverage and depth from positions 81 to 7914. The minor nucleotide population of 25% (48) and read depth of 200$\times$ were used for identifying sites having minor variants. Sequential variants located at the upstream and downstream VP1/2A junction resulted from reverse complemented sequences in NGS reads for reasons as yet unknown, and some variants at the 5′ and 3′ end of the nanoluciferase gene were the result of VP4 reads being mapped to this region, leading to artifacts. Variants in these regions were excluded in the identification of minor variants.

Ethics statement. All animal experiments were conducted in accordance with the policies and procedures set forth by the Guide for the Care and Use of Laboratory Animals of the National Institutes of Health. The Chang Gung University Review Committee (approval no. CGU107-295) and the Institutional

Animal Care and Use Committees of the National Taiwan University College of Medicine and College of Public Health (approval no. 20180425) approved all procedures.

ACKNOWLEDGMENTS

We thank Satoshi Koike of the Tokyo Metropolitan Institute of Medical Science, Japan, for providing hSCARB2 Tg10 mice and Jen-Ren Wang at National Cheng Kung University, Taiwan, for providing infectious clone plasmids EV-A71/MP4 and EV-A71/4643. We also thank Hsiu-Ming Shih and Mi-Hua Tao at Academia Sinica, Taiwan, for setting up the IVIS equipment.

REFERENCES

1. Huang PN, Shih SR. 2014. Update on enterovirus 71 infection. Curr Opin Virol 5:98–104. https://doi.org/10.1016/j.coviro.2014.03.007.
2. Ho M. 2000. Enterovirus 71: the virus, its infections and outbreaks. J Microbiol Immunol Infect 33:205–216.
3. Lum LC, Wong KT, Lam SK, Chua KB, Goh AY, Lim WL, Ong BB, Paul G, AbuBakar S, Lambert M. 1998. Fatal enterovirus 71 encephalomyelitis. J Pediatr 133:795–798. https://doi.org/10.1016/s0022-3476(98)70155-6.
4. Weng KF, Chen LL, Huang PN, Shih SR. 2010. Neural pathogenesis of enterovirus 71 infection. Microbes Infect 12:505–510. https://doi.org/10.1016/j.micinf.2010.03.006.
5. Wang YF, Chou CT, Lei HY, Liu CC, Wang SM, Yan JJ, Su IJ, Wang JR, Yeh TM, Chen SH, Yu CK. 2004. A mouse-adapted enterovirus 71 strain causes neurological disease in mice after oral infection. J Virol 78:7916–7924. https://doi.org/10.1128/JVI.78.15.7916-7924.2004.
6. Huang SW, Wang YF, Yu CK, Su IJ, Wang JR. 2012. Mutations in VP2 and VP1 capsid proteins increase infectivity and mouse lethality of enterovirus 71 by virus binding and RNA accumulation enhancement. Virology 422:132–143. https://doi.org/10.1016/j.virol.2011.10.015.
7. Caine EA, Moncla LH, Ronderos MD, Friedrich TC, Osorio JE. 2016. A single mutation in the VP1 of enterovirus 71 is responsible for increased virulence and neurotropism in adult interferon-deficient mice. J Virol 90:8592–8604. https://doi.org/10.1128/JVI.01370-16.
8. Khong WX, Yan B, Yeo H, Tan EL, Lee JJ, Ng JK, Chow VT, Alonso S. 2012. A non-mouse-adapted enterovirus 71 (EV71) strain exhibits neurotropism, causing neurological manifestations in a novel mouse model of EV71 infection. J Virol 86:2121–2131. https://doi.org/10.1128/JVI.06103-11.
9. Liou AT, Wu SY, Liao CC, Chang YS, Chang CS, Shih C. 2016. A new animal model containing human SCARB2 and lacking stat-1 is highly susceptible to EV71. Sci Rep 6:31151. https://doi.org/10.1038/srep31151.
10. Liao CC, Liou AT, Chang YS, Wu SY, Chang CS, Lee CK, Kung JT, Tu PH, Yu YY, Lin CY, Lin JS, Shih C. 2014. Immunodeficient mouse models with different disease profiles by in vivo infection with the same clinical isolate of enterovirus 71. J Virol 88:12485–12499. https://doi.org/10.1128/JVI.00692-14.
11. Fujii K, Nagata N, Sato Y, Ong KC, Wong KT, Yamayoshi S, Shimanuki M, Shitara H, Taya C, Koike S. 2013. Transgenic mouse model for the study of enterovirus 71 neuropathogenesis. Proc Natl Acad Sci U S A 110:14753–14758. https://doi.org/10.1073/pnas.1217563110.
12. Lin YW, Yu SL, Shao HY, Lin HY, Liu CC, Hsiao KN, Chitra E, Tsou YL, Chang HW, Sia C, Chong P, Chow YH. 2013. Human SCARB2 transgenic mice as an infectious animal model for enterovirus 71. PLoS One 8:e57591. https://doi.org/10.1371/journal.pone.0057591.
13. Zhou S, Liu Q, Wu X, Chen P, Wu X, Guo Y, Liu S, Liang Z, Fan C, Wang Y. 2016. A safe and sensitive enterovirus A71 infection model based on human SCARB2 knock-in mice. Vaccine 34:2729–2736. https://doi.org/10.1016/j.vaccine.2016.04.029.
14. Caine EA, Osorio JE. 2017. In vivo imaging with bioluminescent enterovirus 71 allows for real-time visualization of tissue tropism and viral spread. J Virol 91:e01759-16. https://doi.org/10.1128/JVI.01759-16.
15. Zhang H, Song Z, Zou J, Feng Y, Zhang J, Ren L, Zhang X, Hu Y, Yuan Z, Yi Z. 2020. An infectious clone of enterovirus 71(EV71) that is capable of infecting neonatal immune competent mice without adaptive mutations. Emerg Microbes Infect 9:427–438. https://doi.org/10.1080/22221751.2020.1729665.
16. Wang YF, Yu CK. 2014. Animal models of enterovirus 71 infection: applications and limitations. J Biomed Sci 21:31. https://doi.org/10.1186/1423-0127-21-31.
17. Liu ML, Lee YP, Wang YF, Lei HY, Liu CC, Wang SM, Su IJ, Wang JR, Yeh TM, Chen SH, Yu CK. 2005. Type I interferons protect mice against enterovirus 71 infection. J Gen Virol 86:3263–3269. https://doi.org/10.1099/vir.0.81195-0.
18. Shen FH, Shen TJ, Chang TM, Su IJ, Chen SH. 2014. Early dexamethasone treatment exacerbates enterovirus 71 infection in mice. Virology 464–465:218–227. https://doi.org/10.1016/j.virol.2014.07.021.
19. Yamayoshi S, Yamashita Y, Li J, Hanagata N, Minowa T, Takemura T, Koike S. 2009. Scavenger receptor B2 is a cellular receptor for enterovirus 71. Nat Med 15:798–801. https://doi.org/10.1038/nm.1992.
20. Lancaster KZ, Pfeiffer JK. 2010. Limited trafficking of a neurotropic virus through inefficient retrograde axonal transport and the type I interferon response. PLoS Pathog 6:e1000791. https://doi.org/10.1371/journal.ppat.1000791.
21. Cho H, Kelsall BL. 2014. The role of type I interferons in intestinal infection, homeostasis, and inflammation. Immunol Rev 260:145–167. https://doi.org/10.1111/imr.12195.
22. Dutta S, Sengupta P. 2016. Men and mice: relating their ages. Life Sci 152:244–248. https://doi.org/10.1016/j.lfs.2015.10.025.
23. Schmidt NJ, Lennette EH, Ho HH. 1974. An apparently new enterovirus isolated from patients with disease of the central nervous system. J Infect Dis 129:304–309. https://doi.org/10.1093/infdis/129.3.304.
24. Chen MF, Shih SR. 2016. Motor coordination and balance measurements reveal differential pathogenicity of currently spreading enterovirus 71 strains in human SCARB2 transgenic mice. J Gen Virol 97:3243–3247. https://doi.org/10.1099/jgv.0.000640.
25. Yan JJ, Su IJ, Chen PF, Liu CC, Yu CK, Wang JR. 2001. Complete genome analysis of enterovirus 71 isolated from an outbreak in Taiwan and rapid identification of enterovirus 71 and coxsackievirus A16 by RT-PCR. J Med Virol 65:331–339. https://doi.org/10.1002/jmv.2038.
26. Meng T, Kwang J. 2014. Attenuation of human enterovirus 71 high-replication-fidelity variants in AG129 mice. J Virol 88:5803–5815. https://doi.org/10.1128/JVI.00289-14.
27. Pfeiffer JK, Kirkegaard K. 2005. Increased fidelity reduces poliovirus fitness and virulence under selective pressure in mice. PLoS Pathog 1:e11. https://doi.org/10.1371/journal.ppat.0010011.
28. Vignuzzi M, Stone JK, Arnold JJ, Cameron CE, Andino R. 2006. Quasispecies diversity determines pathogenesis through cooperative interactions in a viral population. Nature 439:344–348. https://doi.org/10.1038/nature04388.
29. Pfeiffer JK, Kirkegaard K. 2006. Bottleneck-mediated quasispecies restriction during spread of an RNA virus from inoculation site to brain. Proc Natl Acad Sci U S A 103:5520–5525. https://doi.org/10.1073/pnas.0600834103.
30. Kuss SK, Etheredge CA, Pfeiffer JK. 2008. Multiple host barriers restrict poliovirus trafficking in mice. PLoS Pathog 4:e1000082. https://doi.org/10.1371/journal.ppat.1000082.
31. McCune BT, Lanahan MR, tenOever BR, Pfeiffer JK. 2020. Rapid dissemination and monopolization of viral populations in mice revealed using a panel of barcoded viruses. J Virol 94:e01590-19. https://doi.org/10.1128/JVI.01590-19.
32. Barreto de Albuquerque J, Silva Dos Santos D, Stein JV, de Meis J. 2018. Oral versus intragastric inoculation: similar pathways of trypanosoma cruzi experimental infection? From target tissues, parasite evasion, and immune response. Front Immunol 9:1734. https://doi.org/10.3389/fimmu.2018.01734.
33. Pfeiffer JK. 2010. Innate host barriers to viral trafficking and population diversity: lessons learned from poliovirus. Adv Virus Res 77:85–118. https://doi.org/10.1016/B978-0-12-385034-8.00004-1.
34. Ohka S, Igarashi H, Nagata N, Sakai M, Koike S, Nochi T, Kiyono H, Nomoto A. 2007. Establishment of a poliovirus oral infection system in human poliovirus receptor-expressing transgenic mice that are deficient in alpha/beta interferon receptor. J Virol 81:7902–7912. https://doi.org/10.1128/JVI.02675-06.

35. Shih C, Liao CC, Chang YS, Wu SY, Chang CS, Liou AT. 2018. Immunocompetent and immunodeficient mouse models for enterovirus 71 pathogenesis and therapy. Viruses 10:674. https://doi.org/10.3390/v10120674.
36. Cox JA, Hiscox JA, Solomon T, Ooi MH, Ng LFP. 2017. Immunopathogenesis and virus-host interactions of enterovirus 71 in patients with hand, foot and mouth disease. Front Microbiol 8:2249. https://doi.org/10.3389/fmicb.2017.02249.
37. Nishimura Y, Shimojima M, Tano Y, Miyamura T, Wakita T, Shimizu H. 2009. Human P-selectin glycoprotein ligand-1 is a functional receptor for enterovirus 71. Nat Med 15:794–797. https://doi.org/10.1038/nm.1961.
38. Yang SL, Chou YT, Wu CN, Ho MS. 2011. Annexin II binds to capsid protein VP1 of enterovirus 71 and enhances viral infectivity. J Virol 85:11809–11820. https://doi.org/10.1128/JVI.00297-11.
39. Tan CW, Poh CL, Sam IC, Chan YF. 2013. Enterovirus 71 uses cell surface heparan sulfate glycosaminoglycan as an attachment receptor. J Virol 87:611–620. https://doi.org/10.1128/JVI.02226-12.
40. Ren XX, Ma L, Liu QW, Li C, Huang Z, Wu L, Xiong SD, Wang JH, Wang HB. 2014. The molecule of DC-SIGN captures enterovirus 71 and confers dendritic cell-mediated viral trans-infection. Virol J 11:47. https://doi.org/10.1186/1743-422X-11-47.
41. Ang PY, Chong CWH, Alonso S. 2021. Viral determinants that drive enterovirus-A71 fitness and virulence. Emerg Microbes Infect 10:713–724. https://doi.org/10.1080/22221751.2021.1906754.
42. Huang SW, Cheng D, Wang JR. 2019. Enterovirus A71: virulence, antigenicity, and genetic evolution over the years. J Biomed Sci 26:81. https://doi.org/10.1186/s12929-019-0574-1.
43. Huang SW, Huang YH, Tsai HP, Kuo PH, Wang SM, Liu CC, Wang JR. 2017. A selective bottleneck shapes the evolutionary mutant spectra of enterovirus A71 during viral dissemination in humans. J Virol 91:e01062-17. https://doi.org/10.1128/JVI.01062-17.
44. Almond JW. 1987. The attenuation of poliovirus neurovirulence. Annu Rev Microbiol 41:153–180. https://doi.org/10.1146/annurev.mi.41.100187.001101.
45. Chen C, Wang Y, Shan C, Sun Y, Xu P, Zhou H, Yang C, Shi PY, Rao Z, Zhang B, Lou Z. 2013. Crystal structure of enterovirus 71 RNA-dependent RNA polymerase complexed with its protein primer VPg: implication for a trans mechanism of VPg uridylylation. J Virol 87:5755–5768. https://doi.org/10.1128/JVI.02733-12.
46. Koboldt DC, Larson DE, Wilson RK. 2013. Using VarScan 2 for germline variant calling and somatic mutation detection. Curr Protoc Bioinformatics 44:15.4.1–15.4.17. https://doi.org/10.1002/0471250953.bi1504s44.
47. Li H, Handsaker B, Wysoker A, Fennell T, Ruan J, Homer N, Marth G, Abecasis G, Durbin R, 1000 Genome Project Data Processing Subgroup. 2009. The sequence alignment/map format and SAMtools. Bioinformatics 25:2078–2079. https://doi.org/10.1093/bioinformatics/btp352.
48. Gong YN, Chen GW, Yang SL, Lee CJ, Shih SR, Tsao KC. 2016. A next-generation sequencing data analysis pipeline for detecting unknown pathogens from mixed clinical samples and revealing their genetic diversity. PLoS One 11:e0151495. https://doi.org/10.1371/journal.pone.0151495.